

PHOTOIONIZED MIXING LAYER MODELS OF THE DIFFUSE IONIZED GAS

LUC BINETTE^{1,2}, NAHIELY FLORES-FAJARDO², ALEJANDRO C. RAGA³, LAURENT DRISSEN¹ AND CHRISTOPHE MORISSET²
Draft version February 23, 2009

ABSTRACT

It is generally believed that O stars, confined near the galactic midplane, are somehow able to photoionize a significant fraction of what is termed the “diffuse ionized gas” (DIG) of spiral galaxies, which can extend up to 1–2 kpc above the galactic midplane. The heating of the DIG remains poorly understood, however, as simple photoionization models do not reproduce the observed line ratio correlations well or the DIG temperature. We present turbulent mixing layer models in which warm photoionized condensations are immersed in a hot supersonic wind. Turbulent dissipation and mixing generate an intermediate region where the gas is accelerated, heated and mixed. The emission spectrum of such layers are compared with observations of Rand (ApJ 462, 712) of the DIG in the edge-on spiral NGC 891. We generate two sequence of models that fit the line ratio correlations between [S II]/H α , [O I]/H α , [N II]/[S II] and [O III]/H β reasonably well. In one sequence of models the hot wind velocity increases while in the other the ionization parameter and layer opacity increases. Despite the success of the mixing layer models, the overall efficiency in reprocessing the stellar UV is much too low, much less than 1%, which compels us to reject the TML model in its present form.

Subject headings: Line: formation – Hydrodynamics – Turbulence – Galaxies: individual: NGC 891–ISM: lines and bands

1. INTRODUCTION

The vast majority of the free electrons in the ISM of the Milky Way reside in a thick (~ 900 pc scale height) diffuse layer, which fills about 20% of the ISM volume, with a local midplane density of about 0.1 cm^{-3} . Such a phase is now known to be a general feature of external star-forming galaxies, both spirals (e.g., Walterbos 1998; Otte et al. 2001, 2002) and irregulars (e.g., Hunter & Gallagher 1990; Martin 1997). It is referred to as the warm ionized medium (WIM) or the diffuse ionized gas (DIG). For edge-on spirals, only in the more actively star-forming galaxies does the gas manifest itself as a smooth, widespread layer of emission detectable above the H II region layer (Rand 1996). It is generally believed that O stars, confined primarily to widely separated stellar associations near the Galactic midplane, are somehow able to photoionize a significant fraction of the ISM not only in the disk but also within the halo, 1–2 kpc above the midplane. The heating of the WIM or DIG remains poorly understood, however. As shown by Madsen, Reynolds & Haffner (2006), the temperatures of the Galactic WIM is 2000–3000 K higher than that of Galactic H II regions. Interestingly, the ratios of forbidden lines such as [S II], [N II] or [O I] with respect to H α have been shown to anticorrelate with the WIM/DIG H α surface brightness (e.g. Rand 1998, hereafter R98; Madsen, Reynolds & Haffner 2006). The fainter the emission brightness, the higher these ratios become. A similar trend is found with scale height z above the disk in edge-on galaxies. Reynolds et al. (1999: RHT) propose that an increase in gas temperature may suffice to explain

such increase in line ratios. The detailed study by Collins & Rand (2001) of the DIG in four edge-on galaxies suggests, however, that a systematic increase in ionization, at least of the fraction of O⁺⁺, might be required as well to account for the observed trends.

Turbulent mixing layers (hereafter TML) induced by a hot wind is one of the mechanisms considered by R98 to provide supplemental ionization and heating. It allowed the author to satisfactorily reproduce the line ratios observed in the DIG of the edge-on spiral NGC 891 (situated at 9.5 Mpc). In order to obtain a reasonable fit, however, the mixing layer model had to be combined with a varying proportion of matter-bounded photoionized condensations. In this composite model, the photoionization models were taken from J. Sokolowski (more information can be found in Bland-Hawthorn et al. 2001) while the mixing layer calculations were borrowed⁴ from Slavin, Shull & Begelman (1993: hereafter SSB). In the current work, we propose two improvements to the heuristic *composite* model introduced by R98: a) an integrated model: the mixing layer and the matter-bounded photoionized condensations are calculated as a single gas component submitted to an external ionizing flux, b) better turbulence microphysics: rather than considering a single TML temperature given by the geometrical mean of the warm and hot phases, we derive a temperature structure for the TML using the mixing length scheme presented by Cantó & Raga (1991), later implemented in the emission line code MAPPINGS IC (Binette et al. 1999).

The paper is organized as follows. The equations describing a turbulent mixing layer and their implementation in the code MAPPINGS IC are discussed in §2. The results obtained from calculations of the TML structure and of its emission line spectrum are presented in §3 and compared with the line ratios from the DIG of NGC 891.

⁴ In particular, the model of SSB with $v_t=25 \text{ km s}^{-1}$, $\bar{T} = 10^{5.3} \text{ K}$ and depleted gas metallicities.

¹ Département de physique, de génie physique et d’optique & Centre de recherche en astrophysique du Québec, Université Laval, Québec, Qc, G1V 0A6.

² Instituto de Astronomía, Universidad Nacional Autónoma de México, Ap. 70-264, 04510 México, D.F., México.

³ Instituto de Ciencias Nucleares, Universidad Nacional Autónoma de México, Ap. 70-543, 04510 México, D. F., México.

A brief discussion follows in § 4.

2. MODELING TURBULENT MIXING LAYERS

2.1. Previous works on TML

It is not so clear what exactly the difference is between “standard” shock wave heating (i.e., heating and/or ionization due to the passage of a single, well defined shock wave), and the heating that takes place in a compressible, turbulent mixing layer. In particular, it is not entirely clear whether such a turbulent layer actually generates a number of weak shock waves, or whether it has a turbulent cascade ending in turbulent dissipation without the appearance of shock waves.

The initial work on the theory of astrophysical turbulent mixing layers was presented by Kahn (1980) in the context of Herbig-Haro jets. Kahn studied the linear and quadratic perturbation theory of the interface at the edge of a jet flow. The linear theory was studied by a number of authors in considerable detail in the context of extragalactic jets in both the gas dynamic and the magnetohydrodynamic contexts (see, e.g., the review of Bodo 1998). For the radiative Herbig-Haro jet case, numerical simulations have been carried out, e.g., by Rossi et al. (1997) and by Stone, Xu & Hardee (1997). Analytic models based on the standard “turbulent viscosity” approach (with a turbulent viscosity parameterized with a simple, “mixing length” approximation) were computed by Cantó & Raga (1991) and Noriega-Crespo et al. (1996). Also, Dyson et al. (1995), Lizano & Giovannardi (1995) and Taylor & Raga (1995) computed models that included more or less detailed treatments of the chemistry associated with mixing layers. However, these models did not include a proper calculation of the ionization state and line emissivity of the ionized regions of these flows. Binette et al. (1999) adopted the mixing layer scheme developed by Raga & Cantó (1997) and incorporated the ionization evolution of all the species considered and the integration of the full emission line spectrum from the mixing layer. These initial calculations were intended to explain the spectrum from small excitation knots observed in Herbig-Haro objects.

In the context of the interstellar and the intracluster medium, Begelman and Fabian (1990) proposed a prescription for evaluating the temperature of a turbulent mixing layer. In a subsequent work, SSB used the same prescription to calculate the emission line spectrum from such layers. Their model included radiative transfer, which allowed these authors to consider the effect of the ionizing photons emitted by the mixing layer itself. These calculations were used by R98 in his study of the NGC 891 DIG.

For the current work, we adopted the mixing length prescription of Binette et al. (1999), described below. We also incorporated radiative transfer, which will allow us to consider the impact of ionizing photons that originate not only from the internal diffuse field produced by the mixing layer, but from external sources as well, such as the ionizing UV from H II regions.

2.2. A mixing length approach

For simplicity, we assume an infinite plane interface, along which a hot wind of temperature T_w is flowing supersonically with velocity V_w with respect to a static

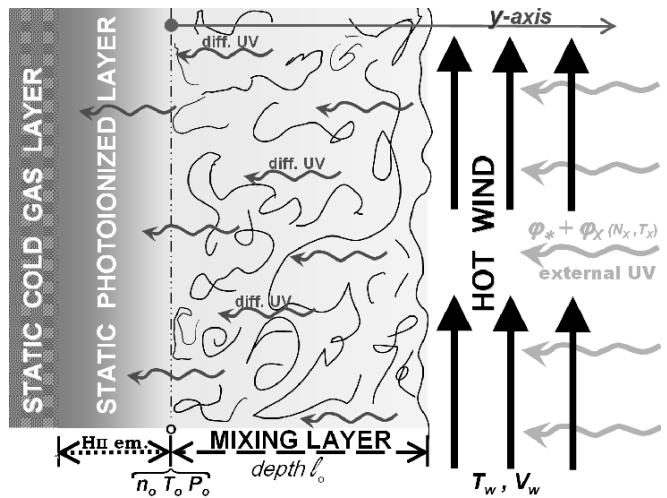


FIG. 1.— Schematic diagram showing the cross-section along the y -axis of a plane-parallel mixing layer of thickness l_o . The x -axis (parallel to the flow) is structure-less in this representation. The mixing layer is formed by the interaction of a supersonic hot wind (of temperature T_w and velocity V_w) with a static layer of warm gas (of H number density n_o and temperature T_o). The gas is entrained into the mixing layer and possess a velocity v , which increases monotonically from $v = 0$ (at $y = 0$) up to V_w . The different layers are all isobaric, with pressure $P_o \approx 2k n_o T_o$. The static layer may contain a photoionized region labeled “H II em.” in the figure. Two sources of ionizing photons can be considered: external UV sources of flux φ_* due to hot stars and the X-ray diffuse field generated by the hot wind φ_X (of column N_X and average temperature T_X). The relative importance of the turbulent and static layers is a free parameter.

warm gas layer of hydrogen number density n_o and temperature T_o . The turbulent mixing layer that develops between the hot and warm phases has a geometrical thickness l_o , as described in the diagram of Fig. 1. For the case of a thin, steady state, high Mach number radiative mixing layer, the advective terms along the direction of the mean flow can be neglected with respect to the corresponding terms across the thickness of the mixing layer (see Binette et al. 2009 for a more detailed description). Under this approximation, the momentum and energy equations can be written as:

$$\mu \frac{d^2 v}{dy^2} = 0, \quad (1)$$

$$\kappa \frac{d^2 T}{dy^2} + \mu \left(\frac{dv}{dy} \right)^2 = L - G, \quad (2)$$

where y is a coordinate measured from the onset of the mixing layer (see Fig. 1), v the bulk flow velocity along the x -axis as a function of y , L and G are the radiative energy loss and gain per unit volume, respectively, and μ and κ are the turbulent viscosity and conductivity, respectively, which are assumed to be constant throughout the cross-section of the mixing layer. Eq.1 can be integrated to obtain the linear Couette flow solution:

$$v(y) = \frac{y}{l_o} V_w, \quad (3)$$

where l_o is the thickness of the TML and V_w the mean velocity of the hot wind (directed parallel to the static warm phase’s surface). This solution can be substituted in Eq. 2, which can then be integrated to derive the temperature cross-section across the layer.

Within the TML, we consider the equations governing the *fractional* abundance f_i of each species i . This

abundance must satisfy the equation:

$$D \frac{d^2 f_i}{dy^2} = S_f^i, \quad (4)$$

where S_f^i is the net sink term (including collisional ionization, radiative and dielectronic recombination, charge transfer... and processes which populate the current species) of the species i . The turbulent diffusivity, D , is of order unity and assumed to be position-independent. At the inner and outer boundaries of the mixing layer, the ionization fractions are set by the equilibrium values.

To complete the description of the mixing layer, we require lateral pressure equilibrium (which determines the density of the flow along the axis y), and calculate the turbulent viscosity with a simple, mixing length parametrization of the form:

$$\mu = \alpha \rho_l c_l l_o, \quad (5)$$

where ρ_l and c_l are the mass density (g cm^{-3}) and sound speed (respectively) averaged⁵ over the cross-section of the mixing layer, l_o is the geometrical thickness of the mixing layer (Fig. 1).

From the work of Cantó & Raga (1991), the value of the proportionality constant α is 0.00247, as clarified in Appendix A. This is the required value for a supersonic mixing layer model to match the opening angle of $\approx 11^\circ$ of subsonic, high Reynolds number laboratory mixing layers in the limit in which the jet Mach number tends to one. Cantó & Raga (1991) also find that mixing layer models with this value for α reproduce the opening angle of mixing layers in jets with Mach numbers⁶, M_w , of up to 20. Our treatment of the TML can be extended to cover the subsonic case by replacing c_l in Eq. 5 by V_w , whenever $V_w < c_l$ (see Appendix A).

Considering that the turbulent conduction and diffusion Prandtl numbers are of order one, we can compute the conduction coefficient as $\kappa \approx \mu c_p$ (where c_p is the heat capacity per unit mass averaged across the mixing layer cross-section) and the diffusion coefficient as $D \approx \mu/\bar{\rho}$. In this way, we obtain a closed set of second order differential equations, Eqs. (2) and (4), which can be integrated with a simple, successive overrelaxation numerical scheme.

2.3. TML calculations with the multipurpose code

MAPPINGS IC

We use the code MAPPINGS IC (Ferruit et al. 1997) to compute the radiative energy loss term L and the photoheating term G (Eq. 2) at each position across the TML. At both the inner and outer boundaries of the mixing layer, we assume equilibrium ionization of the different species, while across the layer, our simple overrelaxation scheme is used to determine the ionization fractions (Eq. 4). For the ion diffusion of each species f_i , the spatial differential equations are converted to temporal equations, with the use of pseudo-time steps $\Delta t = \Delta y^2 l_o / (\alpha \bar{n} c_l)$, where \bar{n} is the average H number density. This allows us to use the temporal algorithm

⁵ The subindex l denotes *averages* across the mixing layer, see Appendix A.

⁶ It is customary to express V_w in terms of the wind Mach number, $M_w = V_w/c_o$, where c_o is the adiabatic sound speed in the static layer.

previously described in Binette & Robinson (1987) for determining the spatial diffusion of the ionic species.

The radiative transfer is determined by integrating (from the hot layer $y = l_o$ down to $y = 0$) the intensity of the UV diffuse field that the layer produces, assuming the *outward only* approximation. Any external UV radiation impinging from the external side is simply added to the diffuse field at the onset of the integration. The intensity of the external ionizing field is defined by the ionization parameter as follows:

$$U_o = \varphi_w / c n_o, \quad (6)$$

where c is the speed of light, φ_w the flux number of ionizing photons impinging on the TML, and n_o , the total H density at $y = 0$. The flux φ_w is the sum of two components: φ_* resulting from external UV sources such as hot stars and φ_X due to the X-ray diffuse field generated by the hot wind (of column N_X and average temperature T_X). The absorption processes that are taken into account in the transfer equations across the TML include all the relevant photoelectric cross-sections of the ions present.

Collins & Rand (2001) used a method based on [N II] $\lambda 6583$ to estimate the gas temperature and, by bootstrapping, they could infer the ionization fractions of N and other species. They find that the hydrogen ionization fraction in NGC 891 is as high⁷ as 0.55–0.80. Because H is fairly ionized and since X-ray ionization is very inefficient in comparison with UV radiation, we infer that their role relative to the soft UV flux from stars must be relatively unimportant. We therefore neglected the term φ_X by setting N_X to a negligible value.

For all the calculations presented in this work, the mixing layers are considered immersed in the radiation field that escapes from H II regions located in the disk. This picture assumes that disk H II regions are on the whole matter-bounded. According to Beckman et al. (2000), Zurita et al. (2002) and Relaño et al. (2002), the fraction of Lyman photons that escape giant H II regions (labeled “leakage fraction” in § 3.2) may lie in the range of 30–50%. The impact of photoionization on our TML model can be inferred from the internal behavior of Γ across the layer, where Γ is defined as follows:

$$\Gamma = \frac{L - G}{L + G}. \quad (7)$$

The quantity Γ is zero when the temperature corresponds to the equilibrium value and tends toward unity when cooling becomes much stronger than heating. In our calculations, we iteratively determine T_o at $y = 0$ until $\Gamma = 0$ is obtained.

After computing the emission line spectrum of a given TML, MAPPINGS IC offers the option of separately computing the emission lines generated by the inner photoionized layer (i.e. $y < 0$ in Fig. 1) where equilibrium ionization prevails. A simple isobaric photoionization model is calculated in this case, using the radiation field that has *not* been absorbed by the mixing layer. The total line spectrum from all the layers is then given by the *sum* of the line intensities from both the TML and the static equilibrium photoionization calculation. For

⁷ Comparable values were inferred for the DIG in the Milky Way by Reynolds et al. (1998) using [O I] $\lambda 6300$.

all the models studied, however, whenever a static photoionized layer was included, it dominated the total spectrum and dwarfed the spectral signature of the turbulent layers. In order to enhance the contribution of the TML and successfully fit the ratios observed in NGC 891, the static equilibrium region must be obviated and the total thickness of the emission layer becomes equal to that given by the turbulent layer alone. This might come about in a 3D geometry if the cold gas were to reside in the core of dense condensations whose *area* is much smaller than that of the surrounding turbulent layers.

Since the mixing layer is isobaric, with pressure P_o , the density profile depends on the behavior of the temperature within the layer itself. The value of P_o is set by two quantities evaluated at the inner TML boundary ($y = 0$): the density n_o and the equilibrium temperature T_o . To be definite, a density of $n_o = 1$ was adopted that applies to all models presented in this work. At such a low density, the *low density regime* fully applies and the calculated line ratios are therefore independent of the actual n_o value used, provided the product $n_o l_o$ is conserved. Our models are appropriate for any density $n_o \lesssim 50$. When the external parameters (U_o , T_w and V_w) are kept constant, TML models turn out to be equivalent whenever the product of the H density n_o and thickness l_o is the same. Therefore, at least in the low density limit regime typical of the DIG, it is sufficient to specify the quantity⁸ $N_o = n_o l_o$ to uniquely define a model.

We found that the temperature of the hot wind is not a critical parameter of the TML models. Its value can be varied and still result in a sequence of equivalent models (i.e. with similar line ratios), provided the value of V_w is kept constant. For this reason, we adopted the same value of $T_w = 8 \times 10^5$ K for all the models presented in this work.

To summarize, in order to compute solutions to the mixing layer, we must first define the external radiation field and then specify the values of the following parameters: the mixing layer's N_o , the ionization parameter, U_o , and finally the velocity of the hot wind, V_w , and its temperature, which we kept constant at 8×10^5 K.

3. MODELING THE DIG IN NGC 891

3.1. The gas abundances

Unless otherwise specified, the abundances of the elements are solar (Anders & Grevesse 1989) and have the following values: (He, C, N, O, Ne, Mg, Si, S, Ca, Ar, Fe) = $[10^5, 363, 112, 851, 123, 38, 36, 16, 2.3, 3.6, 47] \times 10^{-6}$ relative to H (by number). Depleted or oversolar metallicities resulted in line ratios difficult to reconcile with the forbidden line ratios observed in NGC 891.

3.2. The ionizing spectral energy distribution

The first step consists of defining the spectral energy distribution (SED) of the ionizing radiation field *reaching* the DIG. A useful constraint is provided by the observed He I $\lambda 5876$ /H α ratio. In a previous observational work on NGC 891, Rand (1997) measured a ratio of He I $\lambda 5876$ /H $\alpha \approx 0.034$, which he estimated implies

⁸ The quantity N_o is a convenient model descriptor. However, it is a bad estimator of the true integrated H column, which is a lot smaller since the density is not constant but decreases as the temperature rises with thickness y (Fig. 1).

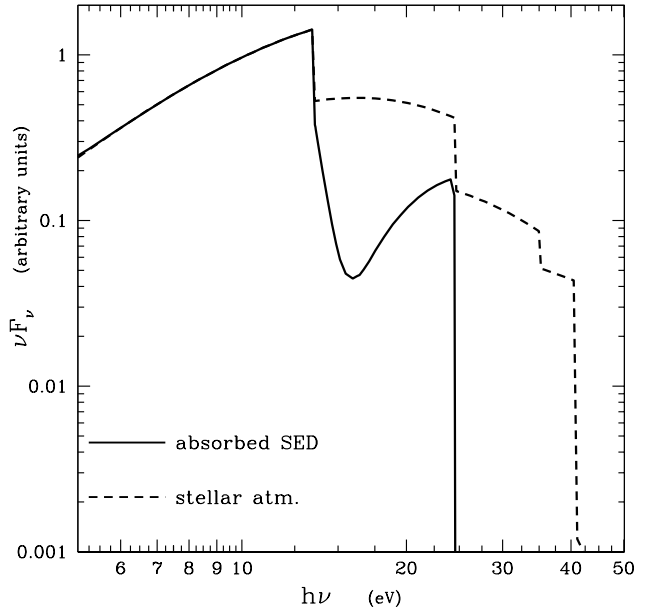


FIG. 2.— The SED of a 38 000 K star (dashed line) as a function of photon energy. The solid line represents the SED of the UV radiation escaping from a matter-bounded photoionized slab that absorbs 80% of the impinging ionizing photons. It is assumed that the DIG is exposed to this absorbed SED.

a ratio of He ionizing photons to H ionizing photons, Q_H/Q_{He} , of about 0.08. To be consistent with this datum, Rand favors a stellar temperature of 37 500 K. In the calculations presented here, we adopt a similar temperature of 38 000 K. The atmosphere models used in MAPPINGS IC are from Hummer & Mihalas (1970). As in R98, we assume that only a fraction of the stellar radiation escapes the H II regions in the spiral disk to reach the DIG. To be definite, we have set the leakage fraction to 20%. To compute this modified SED, we have computed a plane-parallel photoionization model and extracted the photon spectrum at a depth where 80% of the ionizing photons have been used up. The diffuse ionizing radiation from the slab itself has been included. The resulting SED is shown in Fig. 2 (solid line). Because this modified SED contains few ionizing photons beyond 24.6 eV, the mixing layer model presented below is characterized by an He I $\lambda 5876$ /H α ratio as low as $\simeq 0.003$. This suggests a higher stellar temperature for NGC 891 than considered here and in Rand (1997), or a larger leakage fraction than assumed above.

We have verified that the stellar temperature can be raised up to 40 000 K without exceeding the observed He I/H α value (assuming the same leakage fraction). For the DIG in the Milky Way, He I $\lambda 5876$ /H α is observed to be significantly smaller, lying in the range 0.01–0.04 (Madsen et al. 2006).

3.3. TML temperature and ionization structure

In Fig. 3 we present the behavior of the temperature as well as of the imbalance between cooling and heating (Γ , see Eq. 7) as a function of thickness y within a representative mixing layer calculation. For this model, the hot wind velocity is 84 km s^{-1} , while the ionization parameter is $U_o = 10^{-5}$ and the layer's column $N_o = 10^{17} \text{ cm}^{-2}$. The inner boundary is characterized by an equilibrium

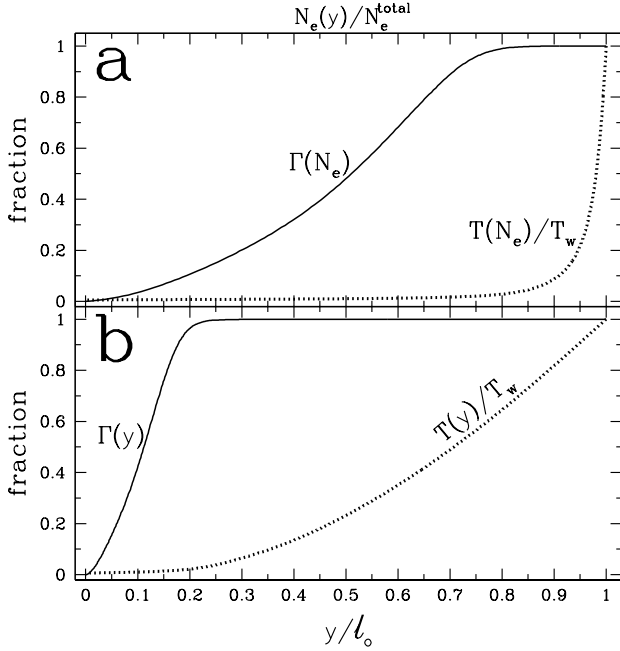


FIG. 3.— Behavior of Γ (Eq. 7) and of the local temperature as a function of (a) the electron column density (normalized to the total value of $1.1 \times 10^{16} \text{ cm}^{-2}$) and of (b) the normalized thickness y/l_o . The model shown has $V_w=85 \text{ km s}^{-1}$, $T_w = 8 \times 10^5 \text{ K}$, $U_o = 10^{-5}$ and $N_o = 10^{17} \text{ cm}^{-2}$. The temperature scale is normalized relative to T_w . The value of the equilibrium temperature, at the onset of the layer, is $T_o=4390 \text{ K}$ (i.e. $T_o/T_w = 0.0055$).

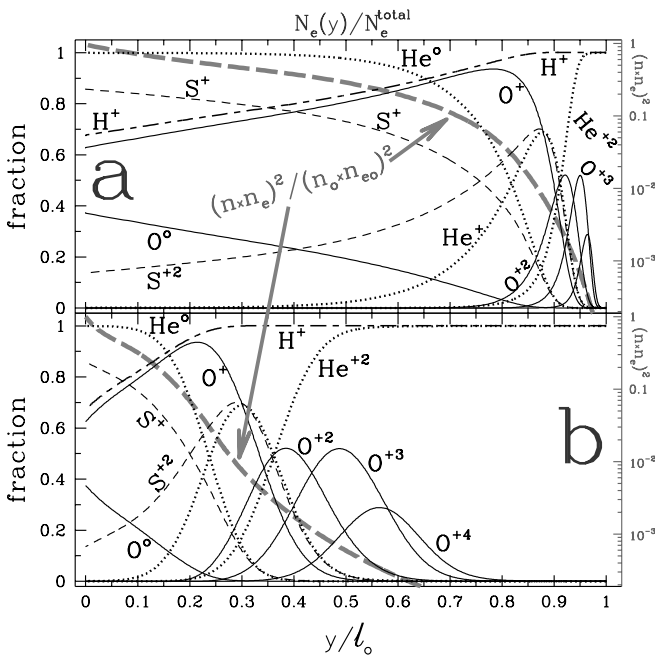


FIG. 4.— Ionization fractions of O, S, He and H for the same model as in Fig. 3 as a function of (a) the electron column density (normalized to the total value of $1.1 \times 10^{16} \text{ cm}^{-2}$) and of (b) the normalized thickness y/l_o . Also shown is the quantity $(n \times n_e)^2$ (thick grey dashed line), which is normalized to the value at $y = 0$ and is plotted on a logarithmic scale, to be read using the rightmost axis. The volume line emissivities from each ion is proportional to this factor. The lines' coding is the same in both panels.

temperature of $T_o = 4390 \text{ K}$. As illustrated in Fig. 3, due to the very hot wind temperature ($T_w \gg T_o$), Γ increases monotonically to reach unity at $y = l_o$ as a result of the cooling term becoming progressively dominant relative to the photoheating term.

The ionization structure within the same TML is shown in Fig. 4. The static layer if it was present would have ionization fractions quite similar to those found at the extreme left in this figure. Line intensities depend on temperature, but scales also with density square. Since the quantity $(n \times n_e)^2$ decreases strongly with increasing thickness (see thick grey dashed line), the local emissivities likewise decrease markedly towards the right. It is therefore apparent that any emission from [O III] or any other species with similar or higher ionization potential are produced in this model only within the mixing layer, and not within the static layer. This would of course be different if a significantly higher stellar temperature was chosen.

3.4. DIG line ratio trends in NGC 891

For comparison with TML models we selected the work of R98 on the DIG in NGC 891. The data on this object present the following advantages: the spectral data are homogeneous, they are of sufficient quality to reveal subtle intrinsic correlations among the line ratios observed at different positions across and along the disk of this edge-on spiral, finally, mid-infrared halo and disk observations with the Spitzer Space Telescope are now available (Rand et al. 2008). We postulate that the line ratio correlations are a direct manifestation of the DIG excitation mechanism rather than positional changes in gas metallicity or in effective stellar temperature.

To optimize the comparison with models, we present the line ratios in Fig. 5 in a format which reveals the essential trends found by R98 in his long slit data. The three ratios [O III]/H β (5007/4861), [O I]/H α (6300/6563) and [N II]/[S II] (6583/6716) are all plotted against the same ratio [S II]/H α (6716/6563). The [O III]/H β line ratio lies below unity in all measurements (panel a). What is most striking about the data is that not only do the forbidden line intensities [O I], [N II] increase along with [S II]/H α , but the high excitation [O III]/H β ratio as well. Such a behavior runs counter to the predictions of simple photoionization models where [O III]/H β increases markedly when the ionization parameter is increased, while the ratios [S II]/H α , [O I]/H α or [N II]/H α all decrease. This leads to the proposition by R98 and Collins & Rand (2001) that another ionization process besides photoionization is likely to be involved. With the Milky Way DIGs, the derived temperatures are found to increase along with the increase of the forbidden lines relative to H α or H β (e.g. Madsen et al. 2006). According to RHT, a systematic temperature increase might be all that is necessary to reproduce the increase in the forbidden line intensities. Again, this runs counter to predictions of simple photoionization models where the temperature is quite insensitive to changes in the value of U_o . Hence various authors have concluded in the existence of a new heating (e.g. RHT) and possibly ionizing mechanism (e.g. R98) in addition to photoionization. For the sake of completeness, we included an inset in Fig. 5 (panel d) where the [N II] temperature computed in models is plotted against [S II]/H α . We may reason-

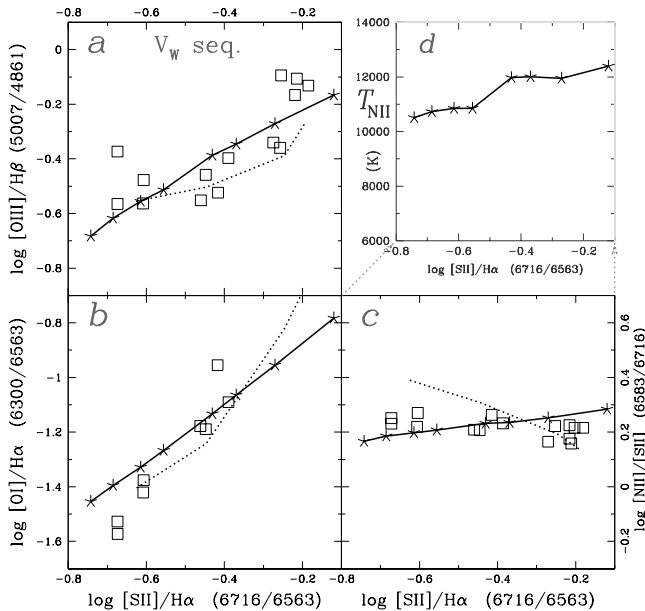


FIG. 5.— Line ratios of (a) $[\text{O III}]/\text{H}\beta$, (b) $[\text{O I}]/\text{H}\alpha$, (c) $[\text{N II}]/[\text{S II}]$ and (d) the T_{NII} temperature, all as a function of the $[\text{S II}]/\text{H}\alpha$ line ratio. Open squares: measurements of R98 of the DIG in NGC 891; continuous line: a sequence of TML models in which V_w is progressively increased by 0.1 dex from 27 to 133 km s^{-1} , while other parameters are kept constant: $N_o = 10^{17} \text{ cm}^{-2}$ and $U_o = 10^{-5}$. The ratio $[\text{S II}]/\text{H}\alpha$ increases with increasing V_w . The dotted line represents a varying mixture of turbulent mixing layers and photoionized matter-bounded models that were proposed by R98.

ably expect that any realistic DIG models should show a significant temperature gradient in such a diagram.

3.5. Specific TML calculations

We carried out an extensive exploration of the parameter space in order to determine the parameter range that could best reproduce the trends present in Fig. 5. As in previous studies, we concur that the layer has to be matter-bounded, otherwise the $[\text{O I}]\lambda 6300/[\text{S II}]\lambda 6716$ ratio would significantly exceed the observed values. Furthermore, for the calculations to show a significant departure from steady-state photoionization as a result of turbulent dissipation and ionization mixing, it required an extremely thin layer, with a column N_o of order $\sim 10^{17} \text{ cm}^{-2}$ only. This raises concerns about the efficiency of turbulent dissipation to contribute significantly to the DIG emission, as discussed in § 4. Because the TML layer in the composite model of R98 was decoupled from the photoionized component, the author was free to adopt a much larger column of $2 \times 10^{18} \text{ cm}^{-2}$ in his matter-bounded photoionization calculations.

A characteristic of the DIG is its relatively weak $[\text{O III}]$ line intensity, which favors relatively small values for the ionization parameter when considering photoionization (e.g. Sokolowski & Bland-Hawthorn 1991). In the case of the composite TML models of R98, the author has employed values that varied between 10^{-5} to 8×10^{-5} . In the TML regime that we have explored, we are lead towards similar values, with U_o typically at $\sim 10^{-5}$. We find that the $[\text{O III}]$ flux is the result of turbulent dissipation rather than of photoionization. On the other hand, low ionization species responsible for lines such as

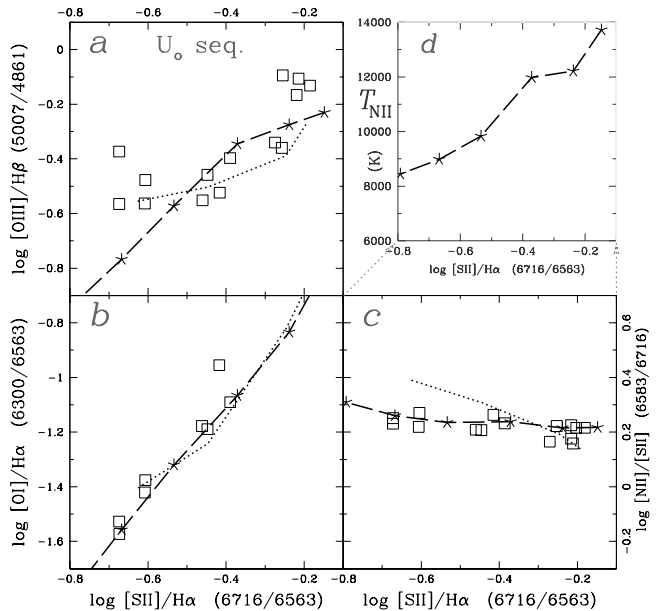


FIG. 6.— Dashed line: a sequence of TML models in which the ionization parameter is progressively increased by 0.2 dex, from 4.0×10^{-6} to 4.0×10^{-5} . The column N_o increases in the same proportion, from 0.4×10^{17} to $4.0 \times 10^{17} \text{ cm}^{-2}$ while V_w is kept constant at 85 km s^{-1} . The ratio $[\text{S II}]/\text{H}\alpha$ decreases with increasing U_o and N_o . Other symbols have the same meaning as in Fig. 5.

$[\text{O II}]$, $[\text{N II}]$, $[\text{S II}]$... are mostly caused by photoionization, but the additional heating due to turbulent dissipation causes these lines to become much brighter. In fact, if a static layer (see Fig. 1) with such a low value of U_o was present behind the TML, the overall line ratios would lie near $[\text{N II}]/[\text{S II}]=0.93$, $[\text{S II}]/\text{H}\alpha=0.087$ and $[\text{O I}]/\text{H}\alpha=0.013$. Therefore, these ratios would all lie outside the boundaries from the three line diagrams *a*, *b* and *c* of Fig. 5. If we relied only on photoionization (without any TML) to fit the observations, we would have to adopt a much harder ionizing SED (but see § 3.2) to provide the necessary heating and the ionization up to O^{+2} .

3.5.1. The V_w -sequence

In Fig. 5, we superpose a sequence of TML models to the data, in which the wind velocity is progressively increased in locked steps, by 0.1 dex, from $V_w = 27$ to 133 km s^{-1} (corresponding to Mach numbers increasing from $M_w=2.53$ to 13.5). The column N_o was set to 10^{17} cm^{-2} and U_o to 10^{-5} . In that sequence, the forbidden line ratios of $[\text{O III}]/\text{H}\beta$ and $[\text{S II}]/\text{H}\beta$ increase with increasing V_w . We note that the temperature inferred from the $[\text{N II}]$ (5755/6583) line ratio, T_{NII} , increases slightly along with $[\text{S II}]/\text{H}\alpha$, as shown in the upper right inset (panel *d*). Overall, the trends in line ratios are well reproduced, better in fact than with the composite (photoionization+TML) model of R98, which is represented by the dotted line. R98 showed that the line ratios not only correlate with decreasing $\text{H}\alpha$ surface brightness, but also with increasing z height above the disk of NGC 891. If the V_w sequence of models were a valid description of the long-slit measurements of R98, this would imply that the wind velocity is increasing with z .

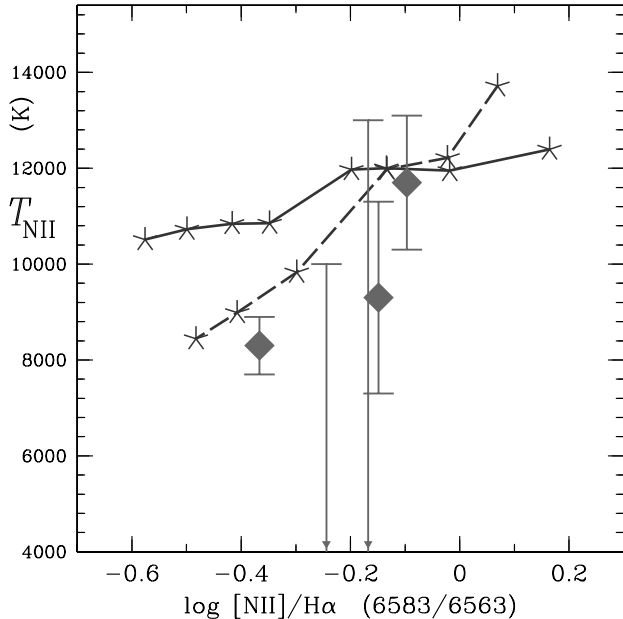


FIG. 7.— The T_{NII} temperature was derived from the temperature sensitive $[\text{N II}]$ (5755/6583) line ratio as a function of the $[\text{N II}]/\text{H}\alpha$ line ratio. The three solid squares correspond to temperatures borrowed from of Madsen et al. (2006) and Reynolds et al. (2001) of the DIG in the Milky Way while the two upper limits correspond to NGC 891 (Rand 1997). Overlaid are the same U_o and V_w sequences of Fig. 5 (solid line) and Fig. 6 (dashed-line), respectively.

3.5.2. The U_o -sequence

Alternatively, it is possible to reproduce the line ratio correlations by varying the ionization parameter instead of V_w . In Fig. 6, we show a sequence of models in which both U_o and N_o increase⁹ in lock steps by 0.2 dex, while V_w is kept constant at 85 km s^{-1} . The initial values of U_o and N_o are 4.0×10^{-6} and $0.4 \times 10^{17} \text{ cm}^{-2}$, respectively, while the final values are 10 times larger. Varying N_o in locked steps with the ionization parameter limits the variations in H I opacity, which is desirable otherwise the TML layers either get too thin or reach a regime in which photoionization takes over. In the sequence shown in Fig. 6, we have ensured that photoionization does not become the dominant process. In fact, $[\text{O III}]$ and the other forbidden lines actually decrease as U_o is increased. For instance, $[\text{O III}]$ gets weaker as U_o increases because the average gas temperature where it is produced *decreases* along the sequence from 51 500 to 40 300 K. This sequence of models shows a $[\text{N II}]$ temperature gradient (Fig. 6d) that is stronger than in the previous sequence (Fig. 5d). When compared to the data on NGC 891, the behavior of the $[\text{O III}]/\text{H}\beta$ ratio is not as closely fit as in the V_w -sequence, but the fit of the other line ratios are better.

3.6. Other DIG observations

Although this study focuses on NGC 891, fitting similar line ratio trends in other objects is certainly achievable. In itself, this does not validate TML models, since the main reason for this is the higher number of free

⁹ Such a sequence is achieved by increasing both quantities φ_w and l_o in lock steps, while keeping n_o constant.

parameters that can be varied and which were already numerous in the alternative case of pure photoionization.

Although forbidden line ratios with respect to $\text{H}\alpha$ or $\text{H}\beta$ increase with height z above the midplane in NGC 891, this behavior is not repeated in all spirals. Cases for instance where $[\text{O III}]/\text{H}\beta$ decreases or reverse trend with height z are well documented in the studies of Miller & Veilleux (2003), Otte et al. (2002) and Collins & Rand (2001). In their studies of face-on M33, Voges & Walterbos (2006) find sudden changes in this ratio. Within the perspective of TML models, these observations bring new constraints to the interpretations that models are able to provide. For instance, in cases where $[\text{O III}]/\text{H}\beta$ decreases with z , we find it improbable that V_w could be decreasing with height, as required by the V_w -sequence (Fig. 5). In the case of the U_o -sequence (Fig. 6), however, a TML interpretation would imply that U_o is increasing with height, which could only come about if the ambient gas pressure decreases faster with z than the local ionizing flux.

The direct measurement of the $[\text{N II}]$ temperature is difficult owing to the intrinsic weakness of the $[\text{N II}]\lambda 5755$ lines. The $[\text{N II}]$ (5755/6583) line ratio has nevertheless been determined in the Milky Way for three DIG sight lines (Madsen et al. 2006; Reynolds et al. 2001). The inferred temperatures are plotted in Fig. 7. The two upper limits for NGC 891, as determined by Rand (1997), are also plotted. The comparison of these three temperatures by Madsen et al. (2006) with those of ‘classical’ H II regions confirms that the DIGs are approximately 2000–3000 K warmer than H II regions. The TML models presented in this work are overlaid in Fig. 7. Despite the scarce data, the comparison with models is encouraging insofar as it shows that turbulent dissipation and mixing can provide the extra heating required by the Galactic DIGs.

With the TML models presented in this work, in which none of the $[\text{O III}]$ emission is the result of photoionization but rather due to turbulent mixing and dissipation, we find that $[\text{O III}]$ is produced at a depth y of very high electron temperature. The behavior of the $[\text{O III}]$ (4363/5007) line ratio in models shows that in both sequences the increase in $[\text{O III}]$ is caused by an increase in average¹⁰ temperature, from $\simeq 40\,000$ to $52\,000$ K. These values are much higher than those characterizing the $[\text{N II}]$ emission zone, to the extent that the $[\text{O III}]\lambda 4363$ line flux is between the value of the $[\text{N II}]\lambda 5755$ flux and half of it. In principle, measuring a high $[\text{O III}]$ temperature or not would provide a strong discriminant for or against TML models.

3.7. The mid-infrared $[\text{Ne II}] 12.81 \mu\text{m}$ and $[\text{Ne III}] 15.56 \mu\text{m}$ lines

Mid-infrared observations of NGC 891 using the Spitzer Space Telescope has been reported by Rand et al. (2008). Of particular interest are the measurements of the $[\text{Ne II}] 12.81 \mu\text{m}$, $[\text{Ne III}] 15.56 \mu\text{m}$ and $[\text{S III}] 18.71 \mu\text{m}$ fluxes of the DIG in the halo (2 measurements) as well as in the disk (1 measurement). Interestingly, the observed

¹⁰ Because of the steep temperature gradient across the TML, the integrated $[\text{O III}]$ (4363/5007) line ratio represents an ‘average’ temperature that is strongly biased towards layers where the gas is densest rather than being close to the temperature where the fraction of O^{+2} peaks (see behavior of $(n \times n_e)^2$ in Fig. 4).

[Ne III]/[Ne II] ratio increases with height z by a factor of three. This is qualitatively similar to the trends revealed by the optical ratios of [S II]/H α or [O III]/H β . Our two TML sequences has [Ne III]/[Ne II] increasing along with [O III]/H β , but the increase is only a factor two. The maximum values reached for the ratio [Ne III]/[Ne II] are 0.067 and 0.070, for the V_w -sequence and U_o -sequence, respectively. This is about 4.5 times too weak with respect to the observed halo value of 0.31. In his analysis, Rand et al. (2008) adopted a Ne/O abundance 2.5 times higher ratio than the solar value (§3.1). Changing our abundance set might resolve this discrepancy.

4. DISCUSSION

A photoionized turbulent mixing layer can reproduce the line ratio trends observed by R98, if it is matter-bounded. Our work confirms the initial intuition of R98 who mixed two causally unrelated ionized components in ad hoc proportions: a TML component and a matter-bounded photoionized component. The main advantage of our integrated model is that the ionized slab considered is submitted in a self-consistent manner to both excitation mechanisms: turbulent dissipation and photoionization. Adjusting the parameters so that the observed line ratios can be reproduced, however, comes at a price. The thickness of the TML layer becomes so small that the overall efficiency in generating emission lines becomes a concern. This can be illustrated as follows. From the definition of U_o , the ionizing photon flux impinging on our putative mixing layer of area A is $3.0 \times 10^4 A n_{-1} U_{-5}$ quanta s^{-1} , where U_{-5} is $U_o/10^{-5}$ and $n_{-1} = n_o/0.1 \text{ cm}^{-3}$. In the case of pure photoionization, assuming ionization equilibrium, the H α luminosity is given by $L_{H\alpha} = 4.44 \times 10^{-8} \eta A n_{-1} U_{-5} \text{ erg s}^{-1}$ where η is a measure of the reprocessing efficiency, that reaches unity in the case of an *ionization-bounded* layer, where all the ionizing photons are absorbed. When the $L_{H\alpha}$ from the TML models are compared to that expected from this simple relationship, we find that the V_w -sequence is characterized by an efficiency η that goes from 0.013 to 0.0031, as V_w is increased. In the case of the U_o -sequence, η goes from 0.0013 to 0.027, as U_o and N_o are increased. What is most problematic, is that the efficiency is lowest when turbulent dissipation is maximized, that is, in the regime where the [O III]/H β ratio is highest, whether we consider the V_w -sequence of Figs. 5 or the U_o -sequence of Fig. 6. The efficiencies at the high [O III]/H β end are only 0.0031 and 0.0013, for the V_w -sequence and U_o -sequence, respectively.

Such an efficiency is uncomfortably low. This can

¹¹ For this particular model, the layer's geometrical thickness is $l_o \simeq 4 \times 10^{17}/n_{-1} \text{ cm}$, which in any case leaves no space for the

be illustrated by using the observations of NGC 891 by Rand (1997). With the long-slit perpendicular to the galactic plane of edge-on NGC 891, the author measured an H α surface brightness of $2 \times 10^{-17} \text{ erg cm}^{-2} \text{ s}^{-1} \text{ arcsec}^{-2}$ at an height $z=2 \text{ kpc}$, where the [O III]/H β ratio peaks. Assuming a distance of $D = 9.5 \text{ Mpc}$ (1 arcsec=46 pc), the slit, perpendicular to the galactic plane, crosses the mid-plane of NGC 891 at 4.6 kpc from the nucleus. We adopt 1'' as the reference spatial scale. We integrate along the thickness of the layer, which we assume extends at most over 9 kpc along the line of sight, so that the layer area A' exposed to the UV flux arising from the midplane becomes $46 \text{ pc arcsec}^{-1} \times 9000 \text{ pc}$. The surface brightness derived from the $L_{H\alpha}$ expression above becomes: $F_{H\alpha} = L_{H\alpha} k A' / (4\pi D^2)$, where k is the number of projected TML layers per arcsec (at $z=2 \text{ kpc}$) along the slit. Hence, $F_{H\alpha} = 1.6 \times 10^{-17} k \eta n_{-1} U_{-5} \text{ erg cm}^{-2} \text{ s}^{-1} \text{ arcsec}^{-2}$. For an efficiency η of 0.0013 and with $U_{-5}=0.4$, matching the observed surface brightness implies the unreasonable number of $k \simeq 2400$ layers¹¹ per arcsec along the slit, assuming a density typical of the DIG in the Milky Way ($n_{-1}=1$). Even if one raises this density by an order of magnitude, too many layers are still required. For higher density values beyond that, there would not be enough O stars to account for the required ionizing flux.

To summarize, it is possible to contrive the values of the parameters describing TML models so that the observed trends in line ratios are reproduced reasonably well. However, the efficiencies of any successful models appear downright too insignificant. In its current form our TML model is therefore invalidated. We may speculate that the gradient in temperature between the hot wind and the warm photoionized gas is so steep that the mixing length approach explored by Cantó & Raga is not directly applicable to the very hot wind surrounding the DIG. Values for the constant α (Eq. 5) about two orders of magnitude larger would be required so that turbulent mixing and dissipation could operate over a layer's thickness much larger than the very small values found in the current model.

One of us, L. D., acknowledges financial support from the Canada Research Chair program and from Canada's Natural Science and Engineering Research Council (NSERC) and from Québec's "Fonds québécois de la recherche sur la nature et les technologies" (FQRNT). This work was supported by the CONACyT grant J-50296. Diethild Starkmeth helped us with proofreading.

hot wind to flow if k is large.

APPENDIX

THE DERIVATION OF CONSTANT α

From Eq. A3 in Cantó & Raga (1991), we obtain that the turbulent viscosity coefficient μ is given by:

$$\mu = \frac{\epsilon}{12} \rho_o c_o l_o, \quad (\text{A1})$$

where ϵ is given by $0.089 \times \text{MIN}[\epsilon_1, \epsilon_2]$ with $\epsilon_1 = \frac{1}{2} \frac{c_o}{c_w}$ and $\epsilon_2 = \frac{1}{3} \frac{c_o}{c_l}$ (see their Eqs. 27, 30 and 36). c_w and c_o correspond to the adiabatic sound speed in the hot wind and in the static layer, respectively. The subindex l denotes *averages* across the mixing layer. Cantó & Raga (1991) refer to the $\epsilon_2 < \epsilon_1$ case as the 'mixing layer limited' case while the 'jet limited' case corresponds to $\epsilon_2 > \epsilon_1$

In the case where $\epsilon_2 < \epsilon_1$, since in the isobaric case $\rho_l c_l^2 = \rho_o c_o^2$, after multiplying the numerator and denominator by $\rho_l c_l$, we can rewrite the above expression as

$$\mu = \frac{0.089}{3 \times 12} \rho_l c_l l_o. \quad (\text{A2})$$

In the notation used in this Paper, the constant α simply corresponds to the ratio $0.089/36 = 0.00247$. In the transonic case or when $\epsilon_1 < \epsilon_2$, we replace c_l in Eq. A2 by $\text{MIN}[V_w, c_l \times \text{MIN}\{1, \frac{3}{2} \frac{c_l}{c_w}\}]$. It turns out that the value of α used by Binette et al. (1999) is a factor 3 too large. This can be corrected by dividing by 3 the values of the layer's thickness, h , quoted in their paper.

REFERENCES

- Anders, E., & Grevesse, N. 1989, *Geochim. Cosmochim. Acta* 53, 197
- Beckman, J. E., Rozas, M., Zurita, A., Watson, R. A., & Knapen, J. H. 2000, *AJ*, 119, 2728
- Begelman, M. C., & Fabian, A. C. 1990, *MNRAS*, 244, 26
- Binette, L., & Robinson A. 1987, *A&A*, 177, 11
- Binette, L., Cabrit, S., Raga, A., & Cantó, J. 1999, *A&A*, 346, 260
- Binette, L., Drissen, L., Úbeda, L., Raga, A.C., Robert, C., Krongold, Y. 2009, *A&A*, in press
- Bland-Hawthorn, J., Freeman, K. C., & Quinn, P. J. 1997, *ApJ*, 490, 143
- Bodo, G.: 1998 in *Astrophysical Jets: Open Problems*, Massaglia S., Bodo G. (eds.), Amsterdam, Gordon and Breach, p. 161
- Cantó, J., & Raga, A. C. 1991, *ApJ*, 372, 646.
- Collins, J. A., & Rand, R. J. 2001, *ApJ*, 551, 57
- Dyson, J. E., Hartquist, T. W., Malone, M. T., & Taylor, S. D. 1995, *RevMexAA (Conf. Series)*, 1, 119
- Ferruit, P., Binette, L., Sutherland, R. S., & Pecontal, E. 1997, *A&A*, 322, 73
- Hummer, D. G., & Mihalas, D. 1970, *MNRAS*, 147, 339
- Hunter, D. A., & Gallagher, J. S., III 1990, *ApJ*, 362, 480
- Kahn, F., 1980, *A&A*, 83, 303
- Lizano, S., Giovanardi, C., 1995, *ApJ* 447, 742
- Madsen, G. J., Reynolds, R. J., & Haffner, L. M. 2006, *ApJ*, 652, 401
- Martin, C. L. 1997, *ApJ*, 491, 561
- Miller, S. T., & Veilleux, S. 2003, *ApJ*, 592, 79
- Noriega-Crespo, A., Garnavich, P.M., Raga, A. C., Cantó, J., Böhm, K. H., 1996, *ApJ* 462, 804
- Otte, B., Reynolds, R. J., Gallagher, J. S., III, & Ferguson, A. M. N. 2001, *ApJ*, 560, 207
- Otte, B., Gallagher, J. S., III, & Reynolds, R. J. 2002, *ApJ*, 572, 823
- Raga, A. C., & Cantó, J.: 1997, in *Molecules in Astrophysics: Probes and Processes*, Van Dishoeck E. (ed.), Dordrecht: Reidel, p. 89
- Rand, R. J. 1996, *ApJ*, 462, 712
- Rand, R. J. 1997, *ApJ*, 474, 129
- Rand, R. J. 1998, *ApJ*, 501, 137 (R98)
- Rand, R. J., Wood, K., & Benjamin, R. A. 2008, *ApJ*, 680, 263
- Relaño, M., Peimbert, M., & Beckman, J. 2002, *ApJ*, 564, 704
- Reynolds, R. J., Hausen, N. R., Tufte, S. L., & Haffner, L. M. 1998, *ApJ*, 494, L99
- Reynolds, R. J., Sterling, N. C., Haffner, L. M., & Tufte, S. L. 2001, *ApJ*, 548, L221
- Reynolds, R. J., Haffner, L. M., & Tufte, S. L. 1999, *ApJ*, 525, L21 (RHT)
- Rossi, P., Bodo, G., Massaglia, S., Ferrari, A. 1997, *A&A*, 321, 672
- Slavin, J. D., Shull, J. M., & Begelman, M. C. 1993, *ApJ*, 407, 83 (SSB)
- Sokolowski, J., & Bland-Hawthorn, J. 1991, *PASP*, 103, 911
- Stone, J.M., Xu, J., Hardee, P. E. 1997, *ApJ*, 483, 136
- Taylor, S. D., Raga, A. C. 1995, *A&A*, 296, 823
- Voges, E. S., & Waltherbos, R. A. M. 2006, *ApJ*, 644, L29
- Waltherbos, R. A. M. 1998, *Publications of the Astronomical Society of Australia*, 15, 99
- Zurita, A., Beckman, J. E., Rozas, M., & Ryder, S. 2002, *A&A*, 386, 801